



Trans. Nonferrous Met. Soc. China 31(2021) 1979-1992

Transactions of Nonferrous Metals Society of China

www.tnmsc.cn



Corrosion and discharge behavior of Mg-xLa alloys (x=0.0-0.8) as anode materials

Yan SONG¹, Hua-bao YANG¹, Yan-fu CHAI¹, Qing-hang WANG¹, Bin JIANG^{1,2}, Liang WU¹, Qin ZOU¹, Guang-sheng HUANG¹, Fu-sheng PAN^{1,2}, Andrej ATRENS³

1. State Key Laboratory of Mechanical Transmissions,

College of Materials Science and Engineering, Chongqing University, Chongqing 400044, China;

- 2. Chongqing Academy of Science and Technology, Chongqing 401123, China;
- 3. School of Mechanical and Mining Engineering, The University of Queensland, Brisbane Old, 4072, Australia

Received 8 July 2020; accepted 7 April 2021

Abstract: The corrosion and discharge performances of binary Mg–xLa (x=0.2–0.8, wt.%) alloys as anode materials for Mg-based batteries were evaluated. Microstructure, hydrogen evolution, mass loss, electrochemical behavior, and half-cell discharge capabilities were characterized. The results show that the corrosion rate of the Mg matrix was decreased by alloying with La, and this could be attributed to the formation of a protective La₂O₃-containing film on the surface of the alloy. The Mg–0.2La alloy displayed the lowest corrosion rate, i.e., 2.4 mm/a in a 3.5 wt.% NaCl solution, Furthermore, the discharge performance of Mg–0.4La alloy was superior to that of pure Mg and other Mg–La alloys; this could be associated with the modified microstructure of the Mg–0.4La alloy, which decreased the self-corrosion and accelerated the detachment of the discharge products.

Key words: Mg-based batteries; Mg-La alloys; corrosion rate; discharge performance

1 Introduction

Development of high-performance anode materials for magnesium (Mg) batteries such as Mg sea-water battery [1,2] and Mg-air battery [3,4] could help combat carbon pollution. Specially, the Mg-air battery, as a type of metal-air batteries [5,6], adopts the oxygen from the atmosphere as the cathode and does not produce the CO2 to the environment. A high-performance Mg-based battery requires an anode with both high discharge potential and high anode efficiency Mg alloys can Theoretically, meet requirements because of their inherent negative electrode potential (-2.37 V vs SHE), high specific energy and high specific capacity [9-11]. The electrolytes typically contain chloride ions [12,13], which also tend to induce corrosion leading to the formation of Mg(OH)₂ as the main corrosion product. Such spontaneous corrosion is an undesirable side reaction, which results in a low utilization efficiency [5,14].

The Mg anode has two intrinsically competing requirements, i.e., stability to corrosion and rapid anodic dissolution. Alloying may reduce the parasitic corrosion loss, which leads to a large energy loss for Mg batteries [8,15]. Among the various elements studied, the rare-earth (RE) elements effectively decreased the corrosion of magnesium [16,17]. Initial studies were focused on the effect of individual REs on the corrosion of binary Mg–RE alloys [18,19]. A decrease in the corrosion rate for small concentrations of RE and

an increase in corrosion for larger concentrations of RE were reported. Furthermore, the corrosion rate of the AM60 alloy was found to decrease by alloying with Ce or La, which can be attributed to the reduced micro-galvanic corrosion and a lower amount of cathodic RE-containing phases [17,20]. Therefore, Mg–RE alloys provide the potential for high values of utilization efficiency as anodes for Mg batteries.

Among the most common RE elements, lanthanum (La) is an environmentally friendly and cost-effective element, which has a more negative standard electrode potential than that of magnesium, i.e., -2.52 V (vs SHE) [21]. La is more anodic than Mg; thus, Mg-La alloys provide discharge voltage lower than that of conventional Mg alloys. The corrosion behavior of an extruded Mg-Al-Pb-La alloy (AP65) has been studied as an anode for a seawater-activated battery [22] and Mg-air battery [23]. The AP65 alloy, a promising anode material with good discharge behavior and high anodic efficiency, contains lead which is harmful to the environment. The influence of alloying Ca, Sm and La with AZ91, on the performance of Mg-air batteries was studied [24]. The combined alloying with Ca, Sm and La was necessary for a high discharge voltage and a low corrosion rate. In prior works, Mg alloys alloyed with La as an additive were studied. Therefore, it is important to identify both the corrosion response and discharge behavior for Mg alloys containing only La as an alloying element.

Mg-La alloy is a promising candidate for anode of Mg batteries; however, there is less systemic research on its self-corrosion and discharge properties in aqueous electrolyte. In this work, Mg-La alloys containing low La content were studied, to define an alloy with the optimum La content that has a low corrosion rate and a rapid anodic dissolution with a high utilization efficiency.

2 Experimental

2.1 Materials

Mg-xLa (x=0.0, 0.2, 0.4, 0.6 and 0.8, wt.%) alloys were melted in an electric resistance furnace. The raw materials included commercially pure Mg (99.9 wt.%) and Mg-20wt.%La master alloy. The furnace was maintained at 720 °C for 30 min to melt the alloy, protected by a flow of 99% CO₂ and 1% SF₆. The molten alloy was adequately stirred and poured into a round (20 mm in diameter) stainless steel mould and preheated to 250 °C. Table 1 presents the chemical compositions of the Mg-xLa alloys determined by inductively coupled plasma-atomic emission spectroscopy (ICP-AES). The composition deviation of La was lower than 0.1 wt.%. Additionally, Fe and Cu, two common impurities in Mg [25,26], were found to be less than 0.005 wt.%, which is below their tolerance limits [27]. Thus, the chemical composition indicated that the alloys were of high-purity.

2.2 Microstructure analysis

The Mg–La alloy samples were successively ground using different grades of SiC abrasive papers and etched using an acetic–picric acid solution to reveal the grain boundaries. The samples were observed using optical microscopy (OM, ZEISS, Axiovert 40 MAT) and scanning electron microscopy (SEM, TESCAN VEGA 3 LMH SEM) of the backscattered electron mode (BSE) and analyzed using energy dispersive spectroscopy (EDS). An X-ray diffractiometer (XRD; D/Max 2500X, Rigaku, Japan) using Cu K_{α} radiation was employed to identify the phase compositions. The scan range of 2θ was from 10° to 80° , and the scan rate was 4 (°)/min.

2.3 Corrosion test

The self-corrosion behaviors of the Mg-La

Table 1 Chemical compositions of Mg-xLa alloys (wt.%)

Material	La	Fe	Cu	Si	Al	Zn	Mn	Mg
Pure Mg	0.0	0.0012	0.0002	0.0039	0.0004	0.0010	0.0011	Bal.
Mg-0.2La	0.1703	0.0025	0.0002	0.0024	_	_	0.0009	Bal.
Mg-0.4La	0.4173	0.0023	0.0002	0.0031	0.0003	0.0001	0.0015	Bal.
Mg-0.6La	0.6061	0.0041	0.0003	0.0051	0.0007	0.0003	0.0025	Bal.
Mg-0.8La	0.8191	0.0047	0.0005	0.0051	0.0014	0.0008	0.0020	Bal.

alloys were examined using an immersion test and electrochemical impedance spectroscopy (EIS). All the measurements were performed in a 3.5 wt.% NaCl solution at the open circuit potential (OCP). The specimens were encapsulated in resin leaving an area of 15 mm × 15 mm exposed to the NaCl solution and were ground using SiC papers up to 2000 grit before exposure to the solution. The immersion test was conducted at ambient temperature using a device described by SONG et al [28], i.e., an inverted funnel and burette assembly was placed above the corroding specimens to collect hydrogen gas. During the tests, the volume of the evolved hydrogen was recorded once every hour. The mass loss of each sample, after immersion for 72 h, was measured after corrosion products were removed ultrasonically by a boiling solution of 200 g/L CrO₃ and 10 g/L AgNO₃, as proposed by WANG et al [29] and CAO et al [30]. The corrosion rate was evaluated as follows [30]:

$$r_c=2.1\Delta m/(S\cdot t_i)$$

where r_c is the corrosion rate (mm·a⁻¹), Δm is the mass loss (mg), S is the surface area (cm²) and t_i is the time of immersion (d). The surfaces after corrosion without the corrosion products were characterized using SEM secondary electron (SE) images. The composition of the corrosion products was identified by XRD analysis of the surfaces of all the alloys after immersion in NaCl solution for 5 h.

EIS was measured using a Princeton PARSTATTM 4000A workstation and a threeelectrode cell. The counter electrode was a platinum sheet with size of 20 mm × 20 mm. The reference electrode was a saturated calomel electrode (SCE). The working electrodes were mounted in resin, leaving an exposed area of 1 cm². Electrochemical impedance spectra were recorded at the OCP after the electrodes had been immersed in the electrolyte for 20 min. The sine perturbation was 5 mV. The measuring frequency range was 100 kHz-0.01 Hz, with 7 points per decade.

2.4 Discharge test

The discharge activity of the electrodes was investigated using a CHI660E electrochemistry workstation with the half-cell method to obtain the discharge curves at constant current density and a

three-electrode cell was employed. The electrolyte was 3.5 wt.% NaCl solution. The surface area of each working electrode exposed to the electrolyte was 10 mm × 10 mm. The potential-time curves were evaluated by applying anodic current densities of 10 and 20 mA/cm² to the working electrodes. After discharge, the anodic efficiency and specific capacity of the Mg-xLa alloys were calculated after removing the discharge products from the surfaces using chromic acid as demonstrated by previous studies [10,31]. The discharged surfaces, with and without discharge products, were recorded using SEM secondary electron (SE) images. An anodic polarization test was also measured in the three-electrode cell system at a scan rate of 1 mV/s after achieving stable open circuit potentials (OCPs).

All the self-corrosion and electrochemical tests were measured in triplicate to ensure good reproducibility and accuracy of the data under identical conditions. The values of all the results reported were the averages of the three tests.

3 Results and discussion

3.1 Microstructures

Figure 1 shows the microstructures of the as-cast Mg-xLa alloys. Mg-La alloys, with low La content (≤0.6 wt.%), had large columnar grains of millimeter-scale length and width. Mg-0.8La had coarse dendrites because of the low solubility of La (approximately 0.74 wt.%) in Mg [32]. These results indicate that the micro-alloying did not refine the grain size of the cast alloys with La. In addition, the interiors of the α -Mg grains of the alloys were decorated with intermetallic compounds, as shown by the backscattered electron (BSE) micrographs, in Fig. 2; while Mg-0.2La had only some fine particles distributing uniformly in the matrix. In addition, Mg-La alloys with La content ≥0.4 wt.% contained rod-like eutectic phases. Increasing the volume fraction of the intermetallic compounds increased the corrosion rate of Mg-RE alloys [19]. The volume fraction of the precipitate phase was evaluated by the Image-Pro Plus 5.0 software, for the BSE images in Fig. 2, and was found to be 0.3%, 1.3%, 3.8% and 5.2% in Mg-0.2La, Mg-0.4La, Mg-0.6La and Mg-0.8La, respectively. amount of the second phase was found to increase

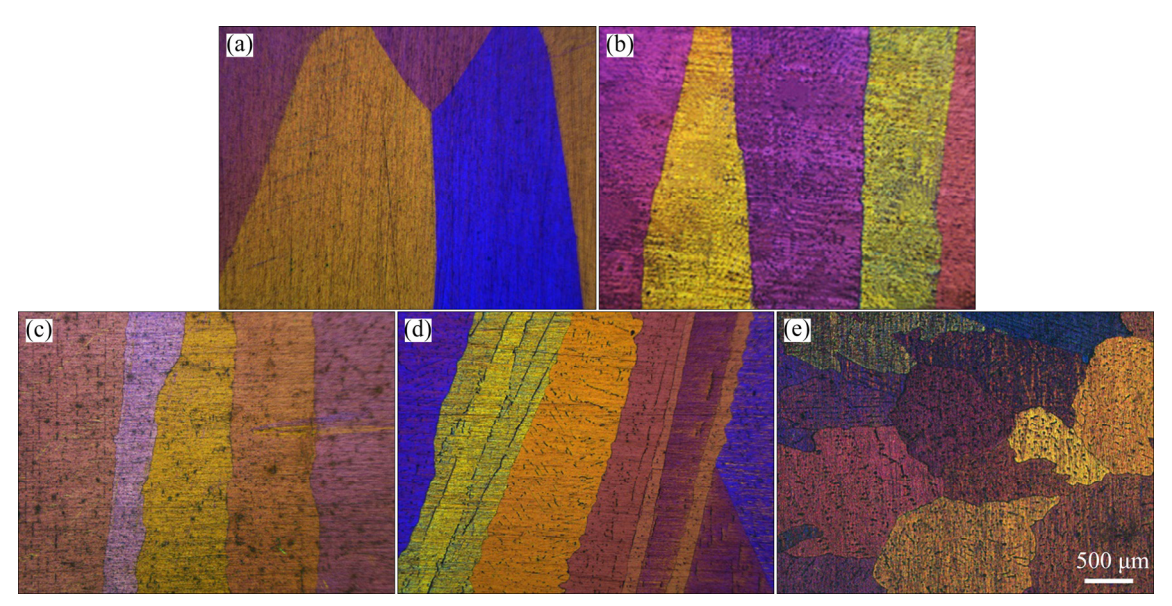


Fig. 1 Optical micrographs of Mg–xLa alloys: (a) Pure Mg; (b) Mg–0.2La; (c) Mg–0.4La; (d) Mg–0.6La; (e) Mg–0.8La

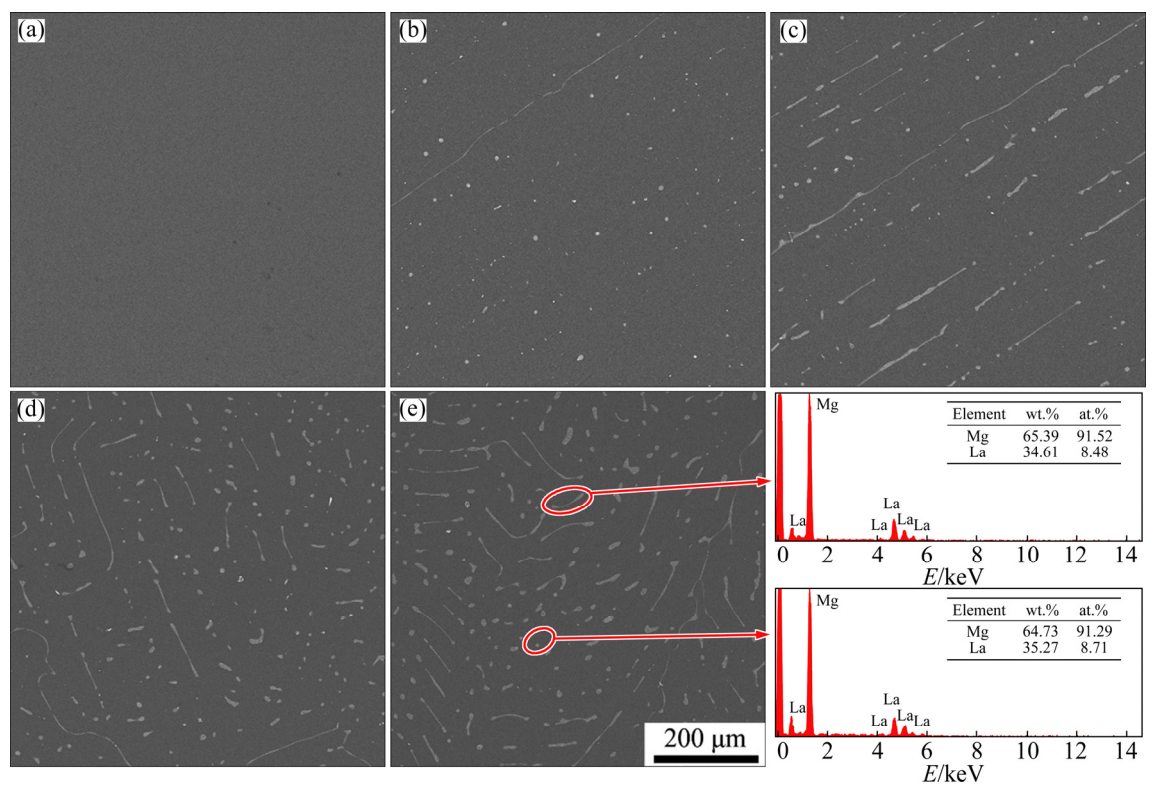


Fig. 2 Backscattered SEM images and EDS spectra of intermetallic compounds: (a) Pure Mg; (b) Mg-0.2La; (c) Mg-0.4La; (d) Mg-0.6La; (e) Mg-0.8La

with increasing La content. The compositions of representative intermetallic compounds in Fig. 2 were analyzed by EDS, all of which corresponded to Mg₁₂La. In addition, XRD patterns qualitatively identified the phase constitution of the Mg–La alloys, as shown in Fig. 3. Only the diffraction

peaks of the α -Mg phase were present for pure Mg, whereas the precipitate phase, Mg₁₂La, was present in the La-containing Mg–La alloys [19]. The intensity of the Mg₁₂La peaks increased with increasing La content, which indicated an increase of Mg₁₂La phase content with increasing La content.

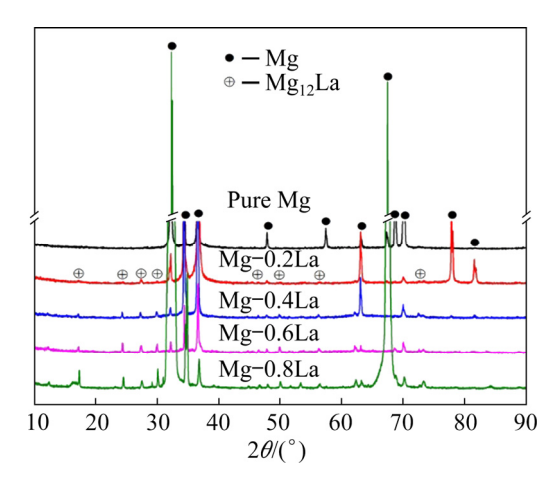
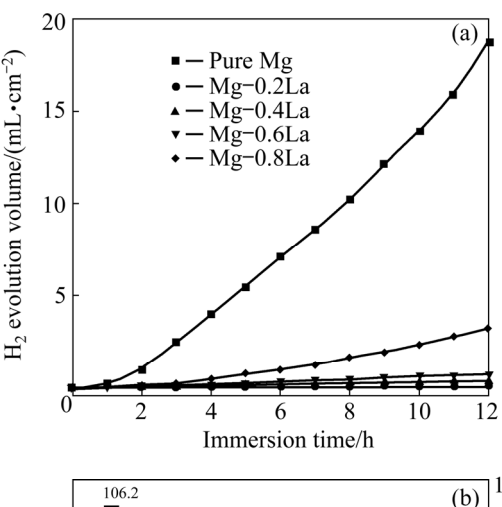


Fig. 3 XRD patterns of Mg-xLa alloys

3.2 Self-corrosion

Hydrogen evolution indicates self-corrosion of the Mg anode in the electrolyte, which is the key factor that decreases the utilization efficiency of an Mg battery during discharge. Therefore, there exists a clear need to investigate the self-corrosion behavior of the Mg anode. The hydrogen evolution curves and the corrosion rates of the Mg anodes are depicted in Fig. 4. Mg-0.2La showed a hydrogen evolution rate much lower than that of pure Mg. However, the hydrogen volume increased at higher content of La (Fig. 4(a)). Figure 4(b) indicates that the hydrogen evolution rate and corrosion rate decreased as the La content increased from 0 to 0.2 wt.%, and increased with further increasing La content. The measured corrosion rate for pure Mg was 122 mm/a, whereas the measured corrosion rate was 2.4 mm/a for Mg-0.2La. Hence, it is proposed that the role of the La alloying was to stifle the hydrogen evolution at Mg, and the optimum La content was found to be less than 0.6 wt.%.

The surface morphologies of specimens after different durations of immersion are presented in Fig. 5 to investigate the dissolution mechanisms of the Mg-xLa alloys. The surface morphologies after exposure in 3.5 wt.% NaCl solution for 5 h are shown in Figs. 5(a-e). Figure 5(a) shows that the reflective surface of the Mg specimen was lost, and extensive damage had spread over the surface. However, there was a lower level of surface attack together with a corrosion product film for the Mg-La alloys with different La contents after immersion in NaCl solution. Additionally, a large proportion of the Mg-0.2La surface remained



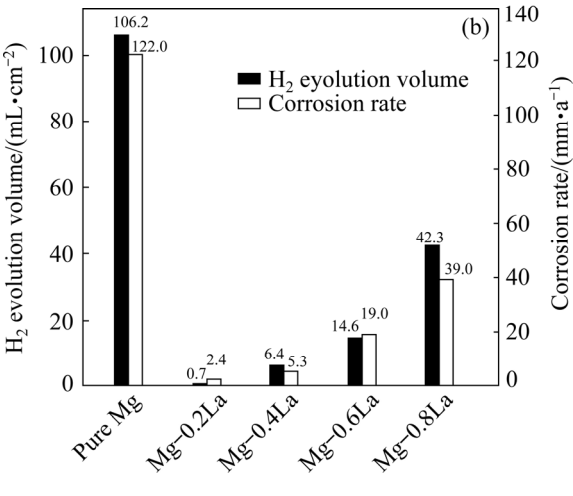


Fig. 4 Data for immersion test in 3.5 wt.% NaCl solution for Mg–xLa alloys: (a) Hydrogen evolution curves in first 12 h; (b) Hydrogen volume and corrosion rate from mass loss over 72 h

unaffected, and there were only a few discrete corrosion sites marked with an ellipse on the surface of the alloy. The density of corrosion sites on the surface of the alloy increased with increasing La content, and localized corrosion appeared when the La content was higher than 0.4 wt.%. This was similar to the trend of increasing the quantity of second phases with increasing La content. After exposure to the NaCl solution for 72 h, the surface of pure Mg was covered with a thick corrosion product film, whereas the surface of Mg-0.2La remained essentially unaffected, indicating that the corrosion film provided good protection. In addition, localized corrosion continued and spread out over the entire specimen when the La content reached 0.8 wt.%.

As previously reported, corrosion in Mg can be effectively decreased in the presence of La [18]. In this work, hydrogen evolution, mass loss, and

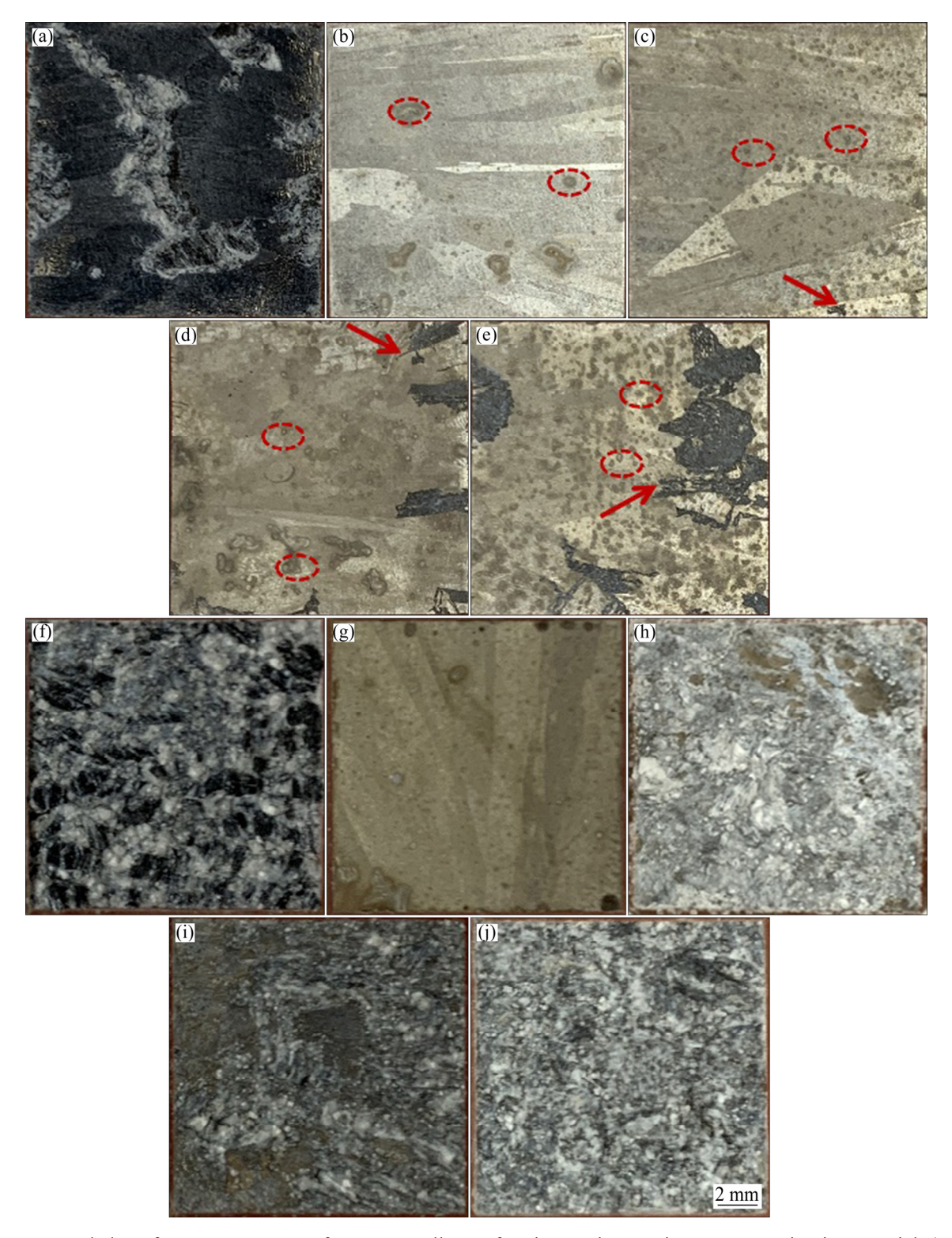


Fig. 5 Corroded surface appearances of Mg–xLa alloys after immersion testing at open circuit potential (OCP) in 3.5 wt.% NaCl solution for 5 h (a–e) and 72 h (f–j): (a, f) Pure Mg; (b, g) Mg–0.2La; (c, h) Mg–0.4La; (d, i) Mg–0.6La; (e, j) Mg–0.8La

surface morphologies indicated that the corrosion rates of the Mg-La alloys were lower than those of pure Mg on immersion for 72 h and could be attributed to the formation of protective films on the

surface of the Mg-La alloys. XRD patterns, as shown in Fig. 6, was employed to investigate the composition of the corrosion products of the Mg-xLa alloys after immersion in NaCl solution

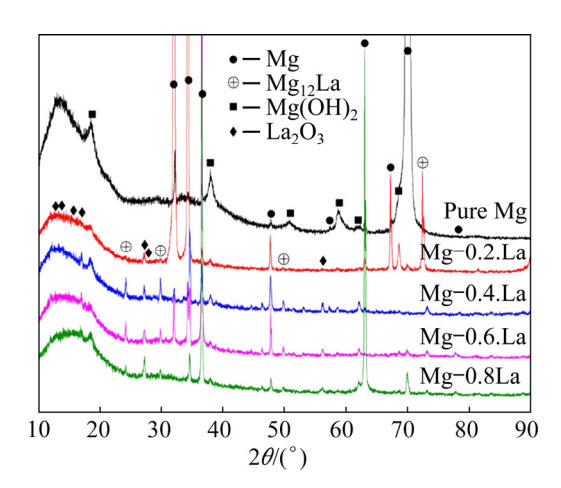


Fig. 6 XRD patterns of surface of Mg–xLa alloys after immersion in 3.5 wt.% NaCl solution for 5 h

for 5 h. There was only one kind of corrosion product, i.e., Mg(OH)₂ (JCPDS PDF No. 44-1482), on the surface of the pure Mg, which can provide some corrosion protection [22], but it is susceptible to be attacked by even small quantities of chloride ions [33]. For the Mg–La alloys, the XRD patterns revealed two phases in the corrosion products. i.e., Mg(OH)₂ and La₂O₃ (JCPDS PDF No. 54-0213). Therefore, it is suggested that the stable La₂O₃, as the corrosion barrier, contributed to the decrease of

the corrosion rate, especially for Mg-0.2La, in which most of the La dissolved into the Mg matrix. Generally, the corrosion of cast metal anodes and the self-peeling of corrosion products are mainly affected by the grain size [10] and second phase particles [13]. As depicted in Fig. 1, with the addition of La, the degree of grain refinement was not significant, but the grain boundaries still increased. These added boundaries were favorable to inhibit hydrogen evolution [34]. As a result, the corrosion resistance of the Mg-La alloys would be improved. Furthermore, the corrosion magnesium alloys was closely associated with the potential difference between the phases, which induced a micro-galvanic reaction [17]. The Mg₁₂La phase is nobler than α -Mg [19], indicating that the intermetallic compound is cathodic and causes galvanic corrosion between the Mg₁₂La phase and α -Mg matrix. Increasing La content increases the volume fraction of the Mg₁₂La phase, which increases the micro-galvanic corrosion. Therefore, increasing La content tends to increase the galvanic corrosion in the Mg-La alloys and thereby increases the corrosion rate.

Figure 7 shows the surface morphologies of these specimens after immersion for 72 h and after

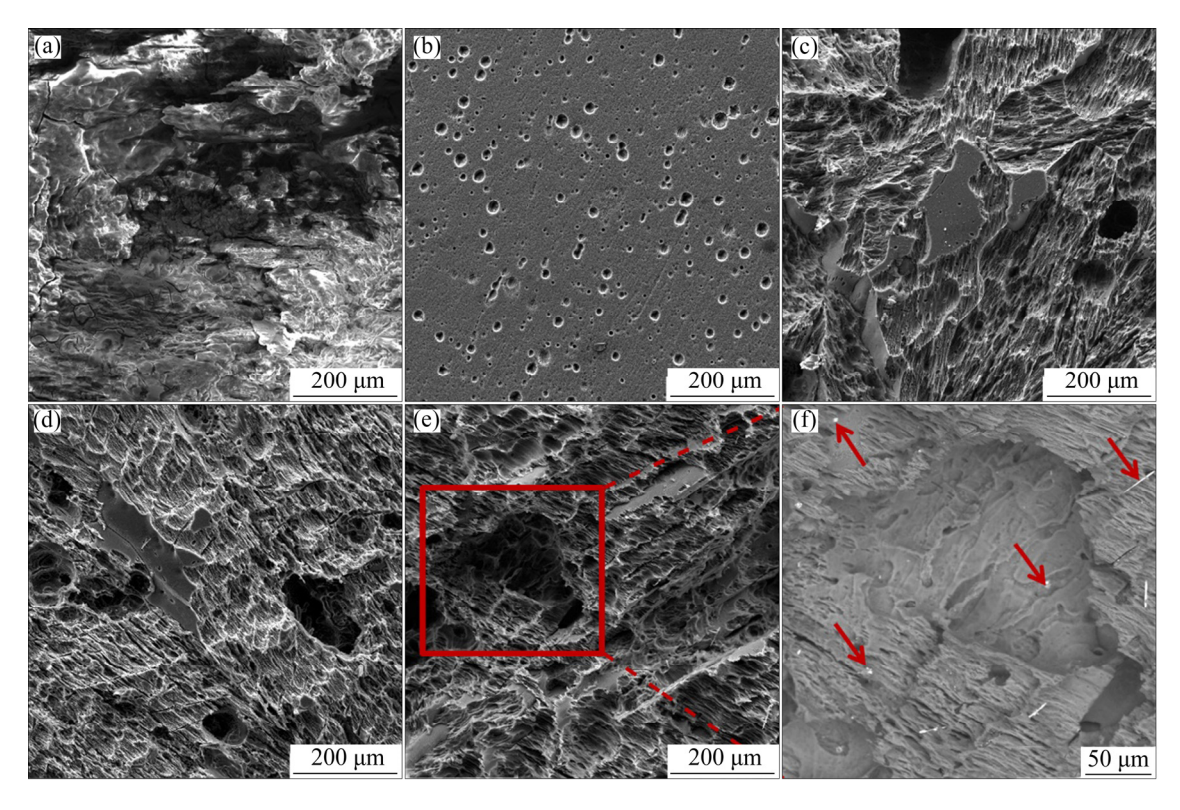


Fig. 7 Surface morphologies of Mg-xLa alloy with corrosion products removed: (a) Pure Mg; (b) Mg-0.2La; (c) Mg-0.4La; (d) Mg-0.6La; (e, f) Mg-0.8La

removal of the corrosion products. The pure Mg suffered serious corrosion with some substantial cavities, as shown in Fig. 7(a), attributed to the absence of any alloying elements which can inhibit the corrosion reactions. The concentration of the impurity phase of Fe, measured by ICP-AES, is given in Table 1. At a mean of 0.0012 wt.% or lower than that in Mg anodes containing La, no corrosion response was observed [9,35]. Therefore, it is reasonable to indicate that Fe or a Fe-rich second phase could be an important site of cathodic hydrogen evolution reaction for pure Mg. Figure 7(b) shows that uniform corrosion with some small corrosion cavities, occurred in Mg-0.2La alloy. The Mg-0.2La alloy showed a lower dissolution rate over the 72 h exposure period, attributed to the protective film which suppressed the propagation of galvanic corrosion. However, Mg–La alloys, with higher La content (≥0.4 wt.%) experienced some localized corrosion, with a number of cavities and bright intermetallic compounds remaining intact, as shown in magnified SEM image with BSE mode in Fig. 7(e). The Mg₁₂La phase particles tend to impart a high tendency for galvanic corrosion, creating a large driving force to damage the surface film. The negative effect caused by Mg₁₂La particles on increasing the corrosion rate was counteracted by the positive effect caused by both the formation of the protective film and the refined grains. Thus, the corrosion rate of the Mg-La alloys increased with La content but was still lower than that of pure Mg.

The self-corrosion performances of the Mg-xLa alloys were also investigated with EIS measurements at the open circuit potential, and the Nyquist plots are shown in Fig. 8. The impedance curves for the as-cast Mg-xLa alloys were characterized by two well-defined capacitive loops. All EIS diagrams were similar with a high-frequency capacitive loop and a low-frequency capacitive loop. The Mg-La alloys exhibited larger

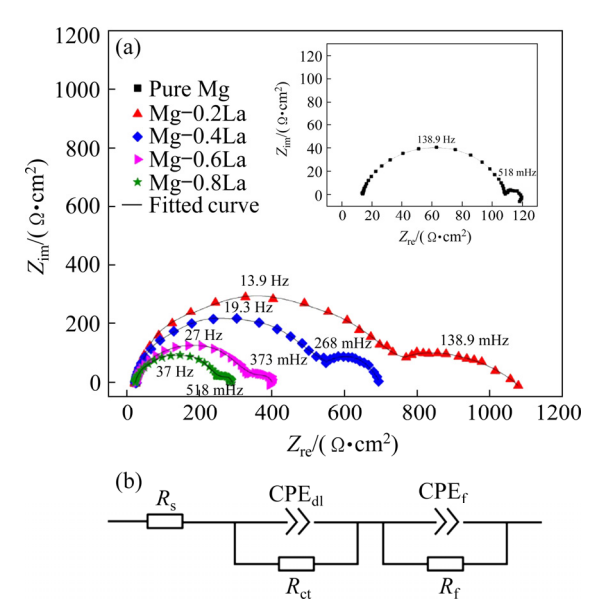


Fig. 8 EIS results of Mg–xLa alloys at OCP in 3.5 wt.% NaCl solution: (a) Nyquist plots; (b) Equivalent circuit after fitting

loops than pure Mg in both high- and lowfrequency regions. The equivalent circuit [22] fitted by the Z-view software is shown in Fig. 8(b), and the fitted values are presented in Table 2. All these curves were fitted well ($\chi^2 < 10^{-3}$). In this equivalent circuit, R_s represents the solution resistance. The first capacitive loop at high frequency is attributed to the charge transfer process at the electrode/ interface, where electrolyte the equivalent component consists of a charge transfer resistance (R_{ct}) parallel to an electric double layer capacitance (CPE_{dl}). The low-frequency capacitive loop is related to the metal oxide film present on the surface of the alloy. The R_f and CPE_f represent corresponding parameters for film resistance and film capacitance, respectively.

In addition, the polarization resistance (R_p) is given by $R_p=R_{ct}+R_f$. A larger R_p value represents a lower corrosion rate of the Mg anode. The value of R_p for Mg-0.2La was larger than that for pure Mg,

Table 2 EIS parameters extracted from Fig. 8 using equivalent circuit

F			e asing rquirus			
Sample	$R_{\rm s}/(\Omega\cdot{\rm cm}^2)$	$R_{\rm ct}/(\Omega\cdot{\rm cm}^2)$	$R_{\rm f}/(\Omega\cdot{\rm cm}^2)$	$CPE_{dl}/(\Omega^{-1}\cdot cm^{-2}\cdot s)$	$CPE_f/(\Omega^{-1}{\cdot}cm^{-2}{\cdot}s)$	χ^2
Pure Mg	14	96	4	2.5×10^{-5}	2.8×10^{-2}	1.8×10^{-4}
Mg-0.2La	24	649	353	1.9×10^{-5}	1.6×10^{-3}	7.7×10^{-4}
Mg-0.4La	25	488	184	2.0×10^{-5}	2.4×10^{-3}	3.9×10^{-4}
Mg-0.6La	24	318	42	4.2×10^{-5}	3.7×10^{-3}	1.9×10^{-4}
Mg-0.8La	24	230	29	3.2×10^{-5}	8.2×10^{-4}	1.3×10^{-4}

and was found to decrease with increasing La content. However, the value was consistently greater for the Mg-La alloys than for pure Mg in this study. These results indicate that a low La content decreased the corrosion rate of the Mg anode in the NaCl solution because of the high value of $R_{\rm f}$. However, the corrosion rate increased with increasing La content, partly due to the decrease of the $R_{\rm f}$, which was greater for all the Mg-La alloys than for pure Mg. This observation is consistent with the mass loss results. In addition, the charge transfer resistance, R_{ct} , also plays an important role during Mg anode dissolution. Figure 8 shows that the behavior of R_{ct} was similar to that of R_f . Alloys with smaller R_{ct} could not be stored in the cell containing electrolyte, while alloys with larger R_{ct} possessed weak discharge activities since the charges could not escape the anode surface easily. Therefore, the alloy with a proper R_{ct} inhibits self-corrosion at the OCP and can provide a negative potential in the course of discharge [36].

3.3 Discharge activity evaluation

Chronopotentiometric responses in a half-cell were used to investigate the discharge activity of the magnesium anodes at anodic current densities of 10 and 20 mA/cm². The discharge potential of the anode was more negative in the half-cell test, which is also in favor of a higher discharge voltage during a full battery test [10]. An imposed current density of less than 20 mA/cm² was used to evaluate the discharge performance of the Mg anode for a long term low-power seawater activated battery and an air battery [29]. Figure 9 depicts the evolution of

the discharge potential for the Mg-xLa alloys. The discharge potentials of all the alloys remained relatively stable during the discharge tests at 10 mA/cm² (see Fig. 9(a)), implying that these alloys exhibited good depolarization during discharge at a small current density. However, a larger current density of 20 mA/cm² increasingly shifted the discharge potential to the positive direction, with increasing duration for each anode (see Fig. 9(b)). In addition, the La content had a significant influence on the discharge potential. The average discharge potentials at 10 and 20 mA/cm² for 1200 s are presented in Table 3. It is shown that all the Mg-La alloys in this study had a more negative discharge potential than pure Mg, even though the potential became less negative with increasing La content. The most negative half-cell potential was achieved by Mg-0.4La at both constant current densities, i.e., -1.601 V (vs Hg/HgCl₂) compared with -1.438 V for pure Mg at 10 mA/cm². In addition, the dissolution behavior of the Mg-La anodes during discharge may be understood from the anodic polarization behavior using the three-electrode half-cell shown in Fig. 10. The Mg-La alloys exhibited different anodic polarization curves. With increasing the potential, the current density of Mg-0.4La increased more rapidly than that of pure Mg and other Mg-La alloys. This result indicates the Mg-0.4La alloy exhibited the most significant anodic dissolution behavior at the imposed anodic polarization. Accordingly, Mg-0.4La was more active not only during galvanostatic discharge but also under anodic polarization. Thus, Mg-0.4La alloy is suitable as the anode for Mg-based battery.

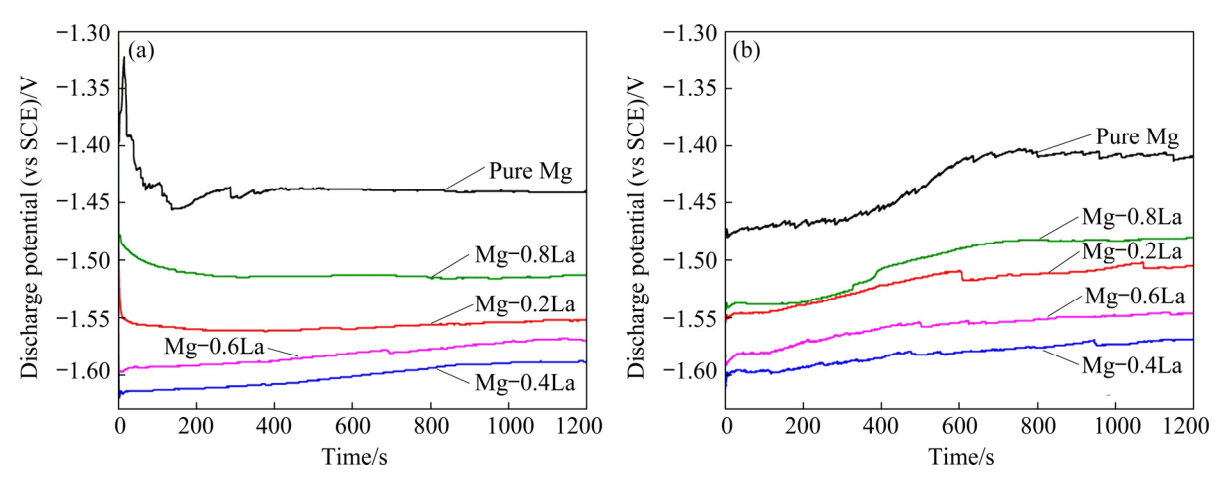


Fig. 9 Galvanostatic discharge curves of Mg-La alloys in 3.5 wt.% NaCl with different current densities: (a) 10 mA/cm²; (b) 20 mA/cm²

Anode —	Average discharge p	potential (vs SCE)/V	Anodic efficiency, η /%		
	10 mA/cm^2 , 1200 s	20 mA/cm ² , 1200 s	10 mA/cm ² , 10 h	20 mA/cm ² , 10 h	
Pure Mg	-1.438	-1.428	40	51	
Mg-0.2La	-1.557	-1.513	66	68	
Mg-0.4La	-1.601	-1.573	60	62	
Mg-0.6La	-1.582	-1.551	54	62	
Mg-0.8La	-1.512	-1.496	52	52	

Table 3 Discharge performances of half-cell with Mg-xLa alloy anodes

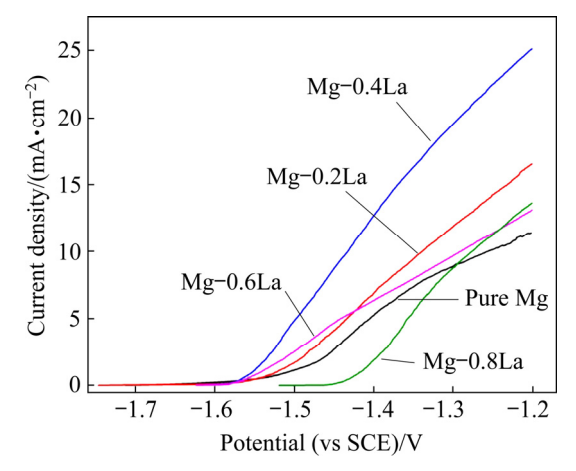


Fig. 10 Anodic polarization curves of Mg–xLa anodes in half-cell

The enhanced discharge potential of the Mg–La alloys was due to the composition and the microstructure. La (-2.52 V vs SHE) is more anodic than Mg (-2.372 V vs SHE). This improved the electrochemical activity of the Mg–La alloys. Thus, the discharge potential of the Mg–La alloys was more negative than that of pure Mg. In addition, the Mg₁₂La particles decreased the spalling resistance of the discharge products [36]. This phenomenon was corroborated by SEM for pure Mg and Mg–La alloys after a half-cell discharge of 10 mA/cm² for 1200 s in Figs. 11(a–e). Generally, the electrochemical reactions of the Mg alloy anode in the NaCl solution can be described by the following reaction mechanisms [1,37]:

$$Mg \rightarrow Mg^{2+} + 2e$$
 (1)

$$Mg^{2+}+2H_2O \rightarrow Mg^{2+}+2OH^-+H_2\uparrow \rightarrow Mg(OH)_2\downarrow +H_2\uparrow \qquad (2)$$

These reactions may appear like the oxidation of Mg during discharge (Eq. (1)) and corrosion (Eq. (2)). However, when the surface of the anode was saturated with Mg²⁺, the precipitation of the main insoluble discharge product, i.e., Mg(OH)₂

occurred, and its deposits were found on the surface of the magnesium electrodes (Eq. (2)). For pure Mg, significant decrease of anodic polarization current density (Fig. 10) occurred when the potential was more positive than -1.35 (vs SCE), implying the rapid deposition of surface product. Accordingly, the surface of pure Mg (Fig. 11(a)) showed a dense deposition of discharge products, which reduced the reaction area between the anode and electrolyte and impeded the discharge. In contrast, the discharge products for the Mg-0.2La alloy were loose, and the Mg substrate was exposed by many microcracks. These phenomena were more pronounced on the surface of Mg-0.4La, which provided an easy contact between the electrode surface and the electrolyte solution. The Mg-0.4La alloy supplied a larger reaction space than pure Mg and Mg-0.2La, thus resulting in negative potentials during the discharge. This result indicates that micro-alloyed La effectively retarded or restricted the occurrence of the reaction shown in Eq. (2). A similar tendency was also observed in the case of self-corrosion resistance. However, for Mg-La alloys with higher La content, the discharge deposits shielding the electrode surface increased gradually because of the rapid conduct of the reaction (Eq. (2)) induced by the increase in the amount of the Mg₁₂La phase, leading to a high diffusion over-potential. The positive effect on the spalling of discharge products caused by the Mg₁₂La phase was counteracted. The increasing La content caused the positive shift of the discharge potential.

The anodic efficiencies of pure Mg and Mg-La alloys, during galvanostatic discharge at 10 and 20 mA/cm², are listed in Table 3. The higher anodic efficiencies imply that more electrons per unit mass were generated under the applied current. Similar to the self-corrosion resistance, the utilization efficiency was improved by the alloying

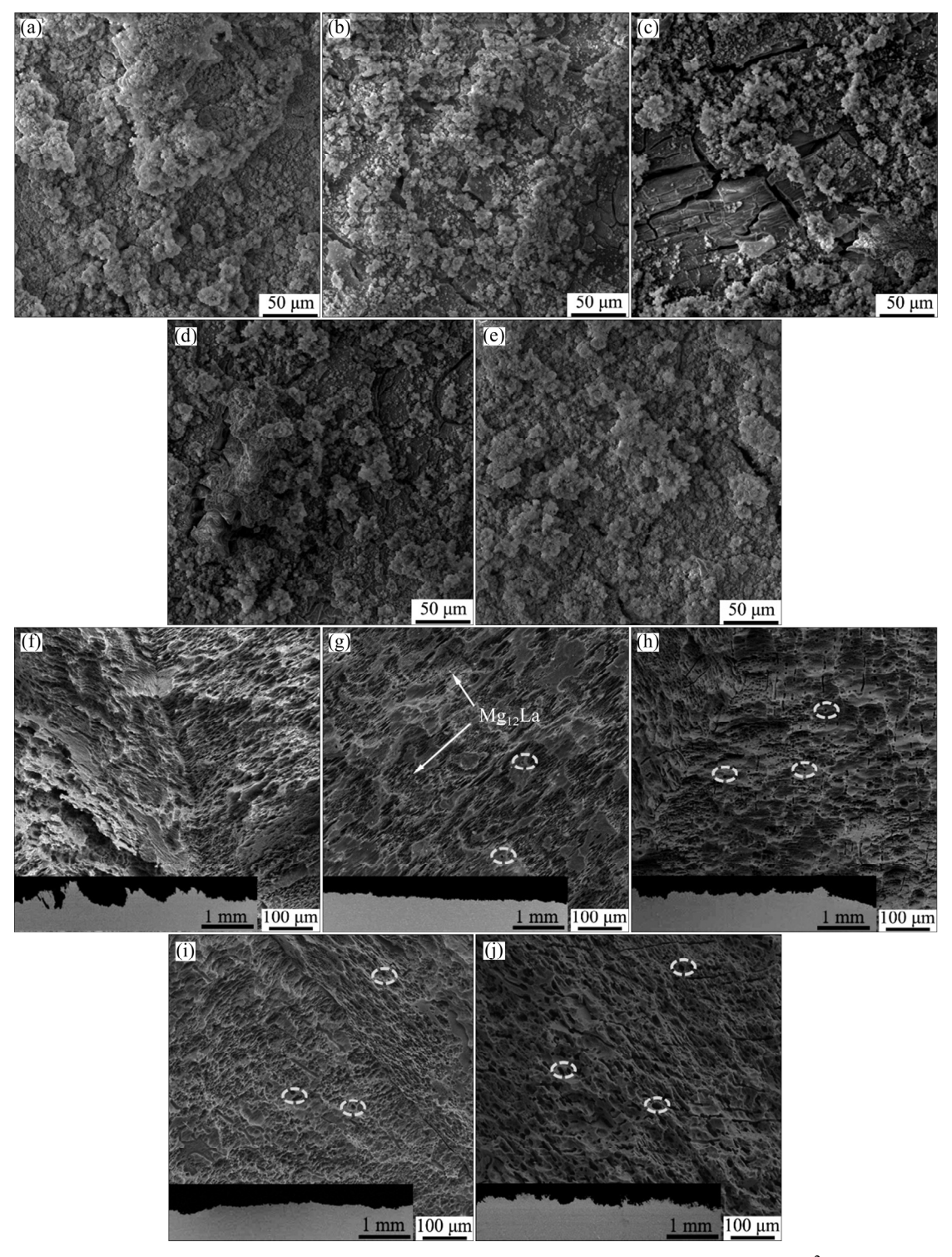


Fig. 11 SEM images of surface of Mg–xLa alloys after discharge at current density of 10 mA/cm² for 1200 s (a–e) and anode surfaces without discharge products discharged at 10 mA/cm² for 10 h (f–j): (a, f) Pure Mg; (b, g) Mg–0.2La; (c, h) Mg–0.4La; (d, i) Mg–0.6La; (e, j) Mg–0.8La (The inserts are corresponding cross sections, where the dark region is the resin and the other is the Mg matrix)

of 0.2 wt.% La, but decreased with the further alloying of La in the Mg–La alloys. For example, Mg–0.2La exhibited the highest utilization efficiencies, i.e., 66% and 69% at 10 and

20 mA/cm², respectively, compared with 41% and 51%, correspondingly, for pure Mg. Furthermore, the efficiency of the Mg-0.4La alloy at 10 mA/cm² also reached 60%, which was higher than that of

the AP65 series alloys [31] and the Mg-Ca binary alloy [10] under the same test condition. One of the factors responsible for the utilization efficiency of magnesium anodes is self-corrosion. The self-corrosion side reactions resulted in low anodic efficiency and supplied no useful energy [38]. This phenomenon is common for all the alloys studied in this work. Therefore, the better self-corrosion resistances of the Mg-La alloys contribute to higher utilization efficiency than pure Mg-0La. Another critical factor which can reduce the utilization efficiency is the "chunk effect", i.e., the detachment of some metallic particles which do not participate in the discharge process.

To investigate the magnitude of the "chunk effect" and understand the dissolution mechanism of the anodes during discharge, the surface and corresponding cross-sections after discharge at 10 mA/cm² for 10 h are presented in Figs. 11(f-g). Figure 11(f) indicated localized and deeply corroded pits in the case of the pure Mg. Such deep pits in the surface of the pure Mg could be said to have resulted from the severe self-corrosion, as shown in Fig. 7(a), leading to the reduction of efficiency. In contrast, anodic the surface morphology of the Mg-0.2La alloy after discharge showed uniform dissolution on both front view and section view during the discharge, with some secondary phases distributing on the surface. Thereby, the utilization efficiency for the Mg-0.2La alloys was less susceptible to the "chunk effect", even though some small cavities (indicated by ellipses) were observed around the second phase on the alloy surface. These cavities were induced by the galvanic corrosion between the Mg matrix and the Mg₁₂La phase. However, after discharge, these cavities increased gradually with an increasing amount of the Mg₁₂La phase, with increasing La content in the Mg-La alloys, leading to the detachment of some metallic pieces [31,39]. Therefore, the discharged surface became rough (see cross-sections in Fig. 11(g)) after the uneven consumption and a suffered severe "chunk effect", leaving many holes in the Mg-0.8La anode as marked by ellipses, which deteriorated the anodic efficiency. Hence, with the self-corrosion resistance and the slight "chunk effect", Mg-La alloys with low La content (≤0.6 wt.%) had higher utilization efficiency, whereas Mg-La alloys with a high La content showed severe self-corrosion and the "chunk effect", resulting in low utilization efficiencies.

4 Conclusions

- (1) The alloying with La decreased the corrosion rate of the Mg-La alloys. This can be attributed to a lower content of Fe-particles and the incorporation of La₂O₃ in the corrosion product film. However, with increasing La content, the protection properties of the surface film on the Mg-La alloys deteriorated. There was an increase in the micro-galvanic corrosion reaction induced by an increasing amount of the intermetallic Mg₁₂La phase; nevertheless, all the Mg-La alloys had corrosion rates less than pure Mg. The lowest corrosion rate, i.e., 2.4 mm/a, was exhibited by the Mg-0.2La alloy.
- (2) The Mg-La alloys displayed better discharge performance than pure Mg at small current densities in the half-cell test, which can be attributed to the higher electrochemical activity of La. The Mg-0.4La anode gave the most negative discharge potential, with an anodic efficiency of 60% at a current density of 10 mA/cm². Therefore, Mg-La alloys with low La content (less than 0.6 wt.%) were attractive candidates of high-performance anode material for the Mg-based battery.

Acknowledgments

The authors are grateful for the financial supports from the National Key Research and Development Program of China (Nos. 2016YFB-0101700, 2016YFB0301104), the National Natural Science Foundation of China (Nos. U1764253, 51971044, U1910213), the National Defense Basic Scientific Research Program of China, the Chongqing Science and Technology Commission, China (Nos. cstc2017zdcy-zdzxX0006, cstc2018jszxcyzdx0082), the Chongqing Scientific Technological Talents Program, China (No. KJXX-2017002), and Qinghai Scientific & Technological Program, China (No. 2018-GX-A1).

References

[1] ZHAO Jun, YU Kun, HU Yan-nan, LI Shao-jun, TAN Xin, CHEN Fu-wen, YU Zhi-ming. Discharge behavior of Mg-4wt.%Ga-2wt.%Hg alloy as anode for seawater activated battery [J]. Electrochimica Acta, 2011, 56:

- 8224-8231.
- [2] WANG Nai-guang, WANG Ri-chu, PENG Chao-qun, FENG Yan, CHEN Bin. Effect of hot rolling and subsequent annealing on electrochemical discharge behavior of AP65 magnesium alloy as anode for seawater activated battery [J]. Corrosion Science, 2012, 64: 17–27.
- [3] HUANG Guang-sheng, ZHAO Yan-chun, WANG Yan-xia, ZHANG Hua, PAN Fu-sheng. Performance of Mg-air battery based on AZ31 alloy sheet with twins [J]. Materials Letters, 2013, 113: 46–49.
- [4] MA Yi-bin, LI Ning, LI De-yu, ZHANG Mi-lin, HUANG Xiao-mei. Performance of Mg-14Li-1Al-0.1Ce as anode for Mg-air battery [J]. Journal of Power Sources, 2011, 196: 2346-2350.
- [5] MA Jing-ling, REN Feng-zhang, WANG Guang-xin, XIONG Yi, LI Ya-qiong, WEN Jiu-ba. Electrochemical performance of melt-spinning Al-Mg-Sn based anode alloys [J]. International Journal of Hydrogen Energy, 2017, 16: 11654–11661.
- [6] MA Jing-ling, ZHANG Yi, QIN Cong-hui, REN Feng-zhang, WNG Guang-xin. Effects of polystyrene sulfonate/graphene and Mn₃O₄/graphene on property of aluminum(zinc)-air batteries [J]. International Journal of Hydrogen Energy, 2020, 45(23): 13025–13034.
- [7] MA Jing-ling, QIN Cong-hui, LI Ya-qiong, REN Feng-zhang, LIU Yong, WANG Guang-xin. Properties of reduced graphene oxide for Mg-air battery [J]. Journal of Power Sources, 2019, 430: 244–251.
- [8] WANG Nai-guang, WANG Ri-chu, PENG Chao-qun, HU Cheng-wang, FENG Yan, PENG Bing. Research progress of magnesium anodes and their applications in chemical power sources [J]. Transactions of Nonferrous Metals Society of China, 2014, 24(8): 2427–2439.
- [9] ZHANG Tian-ran, TAO Zhan-liang, CHEN Jun. Magnesium-air batteries: From principle to application [J]. Materials Horizons, 2014, 1: 196–206.
- [10] DENG Min, HÖCHE D, LAMAKA S V, SNIHIROVA D, ZHELUDKEVICH M L. Mg-Ca binary alloys as anodes for primary Mg-air batteries [J]. Journal of Power Sources, 2018, 396: 109-118.
- [11] HAHN R, MAINERT J, GLAW F, LANG K D. Sea water magnesium fuel cell power supply [J]. Journal of Power Sources, 2015, 288: 26–35.
- [12] XIONG Han-qing, YU Kun, YIN Xiang, DAI Yi-long, YAN Yang, ZHU Hua-long. Effects of microstructure on the electrochemical discharge behavior of Mg-6wt.%Al-1wt.%Sn alloy as anode for Mg-air primary battery [J]. Journal of Alloys and Compounds, 2017, 708: 652–661.
- [13] FENG Yan, XIONG Wen-hui, ZHANG Jun-chang, WANG Ri-chu, WANG Nai-guang. Electrochemical discharge performance of the Mg-Al-Pb-Ce-Y alloy as the anode for Mg-air batteries [J]. Journal of Materials Chemistry A, 2016, 4: 8658-8668.
- [14] MA Jing-ling, WEN Jiu-ba, LI Quan-an, ZHANG Qing. Electrochemical polarization and corrosion behavior of Al–Zn–In based alloy in acidity and alkalinity solutions [J]. Journal of Hydrogen Energy, 2013, 38, 14896–14902.
- [15] ZHENG Tian-xu, HU Yao-bo, ZHANG Yu-xin, YANG Sheng-wei, PAN Fu-sheng. Composition optimization and

- electrochemical properties of Mg-Al-Sn-Mn alloy anode for Mg-air batteries [J]. Materials & Design, 2018, 137: 245-255.
- [16] COY A E, VIEJO F, SKELDON P, THOMPSON G E. Susceptibility of rare-earth-magnesium alloys to microgalvanic corrosion [J]. Corrosion Science, 2010, 52: 3896-3906.
- [17] LIU Wen-juan, CAO Fa-he, CHANG Lin-rong, ZHANG Zhao, ZHANG Jian-qing. Effect of rare earth element Ce and La on corrosion behavior of AM60 magnesium alloy [J]. Corrosion Science, 2009, 51: 1334–1343.
- [18] TAKENAKA T, ONO T, NARAZAKI Y, NAKA Y, KAWAKAMI M. Improvement of corrosion resistance of magnesium metal by rare earth elements [J]. Electrochimica Acta, 2007, 1: 117–121.
- [19] BIRBILIS N, EASTON M A, SUDHOLZ A D, ZHU S M, GIBSON M A. On the corrosion of binary magnesium-rare earth alloys [J]. Corrosion Science, 2009, 51: 683–689.
- [20] LIU Wen-juan, CAO Fa-he, JIA Bing-li, ZHENG Li-yun, ZHANG Jian-qing, CAO Chun-an, LI Xiao-gang. Corrosion behaviour of AM60 magnesium alloys containing Ce or La under thin electrolyte layers. Part 2: Corrosion product and characterization [J]. Corrosion Science, 2010, 52: 639–650.
- [21] SADEGHI A, HASANPUR E, BAHMANI A, SHIN Kwang-seon. Corrosion behaviour of AZ31 magnesium alloy containing various levels of strontium [J]. Corrosion Science, 2018, 141: 117–126.
- [22] SHI Yin-chun, PENG Chao-qun, FENG Yan, WANG Ri-chu, Wang Nai-guang. Microstructure and electrochemical corrosion behavior of extruded Mg-Al-Pb-La alloy as anode for seawater-activated battery [J]. Materials & Design, 2017, 124: 24–33.
- [23] FENG Yan, LEI Ge, HE Yu-qing, WANG Ri-chu, WANG Nai-guang. Discharge performance of Mg-Al-Pb-La anode for Mg-air battery [J]. Transactions of Nonferrous Metals Society of China, 2018, 28: 2274–2286.
- [24] LIU Xuan, XUE Ji-lai, ZHANG Peng-ju, WANG Zeng-jie. Effects of the combinative Ca, Sm and La additions on the electrochemical behaviors and discharge performance of the as-extruded AZ91 anodes for Mg-air batteries [J]. Journal of Power Sources, 2019, 414: 174–182.
- [25] ZHANG Cheng, WU Liang, HUANG Guang-sheng, CHEN Lin, XIA Da-biao, JIANG Bin, ATRENS A, PAN Fu-sheng. Effects of Fe concentration on microstructure and corrosion of Mg-6Al-1Zn-xFe alloys for fracturing balls applications [J]. Journal of Materials Science & Technology, 2019, 35: 2086-2098.
- [26] SONG Guang-lin, ATRENS A. Corrosion mechanisms of magnesium alloys [J]. Advanced Engineering Materials, 1999, 1: 11–33.
- [27] ATRENS ANDREJ, SONG Guang-lin, CAO Fu-yong, SHI Zhi-yong, BOWEN PATRICK K. Advances in Mg corrosion and research suggestions [J]. Journal of Magnesium and Alloys, 2013, 3: 177–200.
- [28] SONG Guang-lin, ATRENS A, STJOHN D. An hydrogen evolution method for the estimation of the corrosion rate of magnesium alloys [J]. Magnesium Technology, 2011: 255–262.
- [29] WANG Nai-guang, MU Yang-chang, XIONG Wen-hui,

- ZHANG Jun-chang, LI Qi, SHI Zhi-cong. Effect of crystallographic orientation on the discharge and corrosion behaviour of AP65 magnesium alloy anodes [J]. Corrosion Science, 2018, 144: 107–126.
- [30] CAO Fu-yong, SHI Zhi-ming, SONG Guang-Ling, LIU Ming, DARGUSCH M S, ATRENS A. Influence of hot rolling on the corrosion behavior of several Mg-X alloys [J]. Corrosion Science, 2015, 90: 176–191.
- [31] WANG Nai-guang, WANG Ri-chu, PENG Chao-qun, PENG Bing, FENG Yan, HU Cheng-wang. Discharge behaviour of Mg-Al-Pb and Mg-Al-Pb-In alloys as anodes for Mg-air battery [J]. Electrochimica Acta, 2014, 149: 193–205.
- [32] BIRBILIS N, CAVANAUGH M K, SUDHOLZ A D, ZHU S M, EASTON M A, GIBSON M A. A combined neural network and mechanistic approach for the prediction of corrosion rate and yield strength of magnesium—rare earth alloys [J]. Corrosion Science, 2011, 53: 168–176.
- [33] ZENG Rong-chang, LIU Zhen-guo, ZHANG Fen, LI Shuo-qi, CUI Hong-zhi, HAN En-hou. Corrosion of molybdate intercalated hydrotalcite coating on AZ31 Mg alloy [J]. Journal of Materials Chemistry A, 2014: 13049–13057.
- [34] ALVAREZ-LOPEZ M, PEREDA M D, del VALLE J A, FERNANDEZ-LORENZO M, GARCIA-ALONSO M C, RUANO O A, ESCUDERO M L. Corrosion behaviour of

- AZ31 magnesium alloy with different grain sizes in simulated biological fluids [J]. Acta Biomaterialia, 2010, 6: 1763–1771.
- [35] BIRBILIS N, WILLIAMS G, GUSIEVA K, SAMANIEGO A, GIBSON M A, MCMURAY H N. Poisoning the corrosion of magnesium [J]. Electrochemistry Communications, 2013, 34: 295–298.
- [36] WANG Nai-guang, WANG Rri-chu, FENG Yan, XIONG Wen-hui, ZHANG Jun-chang, DENG Min. Discharge and corrosion behaviour of Mg-Li-Al-Ce-Y-Zn alloy as the anode for Mg-air battery [J]. Corrosion Science, 2016, 112: 13-24.
- [37] UDHAYAN R, BHATT D P. On the corrosion behaviour of magnesium and its alloys using electrochemical techniques [J]. Journal of Power Sources, 1996, 63: 103–107.
- [38] MA Jing-ling, ZHANG Yi, MA Ming-sheng, QIN Cong-hui, REN Feng-zhang, WANG Guang-xin. Corrosion and discharge performance of a magnesium aluminum eutectic alloy as anode for magnesium-air batteries [J]. Corrosion Science, 2020, 170: 108695.
- [39] YUASA M, HUANG Xin-sheng, SUZUKI K, MABUCHI M, CHINO Y. Discharge properties of Mg-Al-Mn-Ca and Mg-Al-Mn alloys as anode materials for primary magnesium-air batteries [J]. Journal of Power Sources, 2015, 297: 449-456.

Mg-xLa 合金($x=0.0\sim0.8$)阳极材料的腐蚀及放电行为

宋 燕 ¹, 杨华宝 ¹, 柴炎福 ¹, 王庆航 ¹, 蒋 斌 ^{1,2}, 吴 量 ¹, 邹 勤 ¹, 黄光胜 ¹, 潘复生 ^{1,2}, Andrej ATRENS³

- 1. 重庆大学 材料科学与工程学院 机械传动国家重点实验室, 重庆 400044;
 - 2. 重庆科技学院, 重庆 401123;
- 3. School of Mechanical and Mining Engineering, The University of Queensland, Brisbane Qld, 4072, Australia
- 摘 要:研究镁基电池阳极材料 Mg-xLa(x=0.2~0.8,质量分数,%)的腐蚀以及放电行为。观察显微组织并测试析 氢、质量损失、电化学行为以及半电池放电性能。结果表明,镧元素的加入使得镁基体的腐蚀速率下降,主要是 因为表面生成具有氧化镧的保护膜。Mg-0.2La 合金在 3.5%氯化钠溶液中表现出最低的腐蚀速率,即 2.4 mm/a; 同时,Mg-0.4La 合金表现出优于纯 Mg 以及其他 Mg-La 合金的放电性能,这主要是因为 Mg-0.4La 合金具有改善的微观结构,该结构能降低自腐蚀速率,并加速放电产物的脱落。

关键词: 镁基电池; Mg-La 合金; 腐蚀速率; 放电行为

(Edited by Bing YANG)